The Cryosphere, 8, 1457–1468, 2014
www.the-cryosphere.net/8/1457/2014/
doi:10.5194/tc-8-1457-2014

The Cryosphere Open Access

Ice–ocean interaction and calving front morphology at two west Greenland tidewater outlet glaciers

N. Chauché[1], A. Hubbard[1], J.-C. Gascard[2], J. E. Box[3,4], R. Bates[5], M. Koppes[6], A. Sole[7], P. Christoffersen[8], and H. Patton[1]

[1]Department of Geography and Earth Science, Aberystwyth University, Aberystwyth, UK
[2]Laboratoroire d'Océanographie et du Climat, Expérimentation et approche Numérique, Université Pierre et Marie Curie, Paris, France
[3]Byrd Polar Research Center, The Ohio State University, Columbus, Ohio, USA
[4]Geological Survey of Denmark and Greenland, Copenhagen, Denmark
[5]School of Geography and Geosciences, St-Andrews University, St-Andrews, UK
[6]Department of Geography, University of British Columbia, Vancouver, Canada
[7]Department of Geography, University of Sheffield, Sheffield, UK
[8]Scott Polar Research Institute, University of Cambridge, Cambridge, UK

Correspondence to: N. Chauché (noc3@aber.ac.uk)

Received: 5 October 2013 – Published in The Cryosphere Discuss.: 20 November 2013
Revised: 24 May 2014 – Accepted: 12 June 2014 – Published: 8 August 2014

Abstract. Warm, subtropical-originating Atlantic water (AW) has been identified as a primary driver of mass loss across the marine sectors of the Greenland Ice Sheet (GrIS), yet the specific processes by which this water mass interacts with and erodes the calving front of tidewater glaciers is frequently modelled and much speculated upon but remains largely unobserved. We present a suite of fjord salinity, temperature, turbidity versus depth casts along with glacial runoff estimation from Rink and Store glaciers, two major marine outlets draining the western sector of the GrIS during 2009 and 2010. We characterise the main water bodies present and interpret their interaction with their respective calving fronts. We identify two distinct processes of ice–ocean interaction which have distinct spatial and temporal footprints: (1) homogenous free convective melting which occurs across the calving front where AW is in direct contact with the ice mass, and (2) localised upwelling-driven melt by turbulent subglacial runoff mixing with fjord water which occurs at distinct injection points across the calving front. Throughout the study, AW at $2.8 \pm 0.2\,^{\circ}C$ was consistently observed in contact with both glaciers below 450 m depth, yielding homogenous, free convective submarine melting up to ~ 200 m depth. Above this bottom layer, multiple interactions are identified, primarily controlled by the rate of subglacial fresh-water discharge which results in localised and discrete upwelling plumes. In the record melt year of 2010, the Store Glacier calving face was dominated by these runoff-driven plumes which led to a highly crenulated frontal geometry characterised by large embayments at the subglacial portals separated by headlands which are dominated by calving. Rink Glacier, which is significantly deeper than Store has a larger proportion of its submerged calving face exposed to AW, which results in a uniform, relatively flat overall frontal geometry.

1 Introduction and background

The west Greenland current advects deep (> 400 m), warm (> 3 °C) and saline (> 34.8 PSU – practical salinity units) Atlantic water around the south coast of Greenland, transferring large fluxes of thermal energy of a subtropical origin into this sensitive polar environment (Christoffersen et al., 2012; Holland et al., 2008; Kjær et al., 2012; Mortensen et al., 2011; Ribergaard, 2007; Sutherland et al., 2013). The frontal dynamics of tidewater outlet glaciers draining the Greenland Ice Sheet (GrIS) can be profoundly influenced by Atlantic water (AW), which has the potential to directly access their

calving fronts via over-deepened glacial troughs cut through the continental shelf, thereby controlling their energy and mass balance (Hanna et al., 2014; Pfeffer, 2007; Rignot et al., 2010). For example, in west Greenland the sustained attrition of Jakobshavn Isbræ, observed since 1998 (Joughin et al., 2012), has been attributed to warming of subsurface water in Disko Bay and adjacent coastal seas (Holland et al., 2008). Similarly, AW was identified circulating within Sermilik and Kangerdlugssuaq fjords in east Greenland and is implicated in the retreat of Helheim and Kangerdlugssuaq glaciers over the last decade (Straneo et al., 2010, 2011). In NW Greenland, two distinct phases of dynamic ice loss (1985–1990 and 2005–2010) across the Melville Coast have been attributed to oceanic rather than atmospheric forcing (Kjær et al., 2012). An implicit assumption in these studies is that warm AW comes into direct contact with the marine termini of large tidewater outlet glaciers draining the ice sheet (Holland et al., 2008; Kjær et al., 2012; Motyka et al., 2011; Rignot et al., 2010; Straneo et al., 2012). Yet to date few observational studies have been focused on the actual ice–ocean interface, in particular on the specific controls governing submarine melt rates and the concomitant mass and energy exchanges which determine outlet glacier and fjord dynamics alike (Hubbard, 2011).

To date, several processes of interaction between fjord water and tidewater calving fronts have been observed, modelled and/or speculated upon including forced convection caused by buoyant subglacial fresh water (SgFW) discharged at depth and entraining AW as it rises (Jenkins, 2011; Mugford and Dowdeswell, 2011; Salcedo-Castro et al., 2011; Sciascia et al., 2013; Sole et al., 2012; Xu et al., 2012, 2013) as well as wind stress and tide-driven fjord circulation (Mortensen et al., 2011; Sole et al., 2012; Straneo et al., 2010; Sutherland and Straneo, 2012). Furthermore, it is emerging that circulation in Greenland's deep fjords is more complex than the single convective cell (estuarine-like) circulation model that has been assumed previously in energy-mass balance calculations (Motyka et al., 2003; Rignot et al., 2010). For instance, a vertical superposition of convective cells was observed (Straneo et al., 2011; Sutherland and Straneo, 2012) and more recently modelled (Sciascia et al., 2013; Sole et al., 2012) within fjords in east Greenland.

In this study we observe and document the interaction between fjord waters and the calving front at two major outlets – Rink and Store – that drain the western GrIS over two successive, but contrasting, melt years in August 2009 and 2010. The processes of AW-driven submarine melting and subglacial fresh-water-driven upwelling plumes are observed in both fjords. Differences and similarities in the spatial and temporal patterns of these processes are identified and highlighted, demonstrating significant impact and control of subglacial fresh-water runoff and discharge on calving front dynamics and geometry.

2 Field site

Uummannaq Bay is unique on the west coast of Greenland insofar as it has an over-deepened glacial trough to at least ~ 450 m depth, which extends uninterrupted to the continental shelf break (Jakobsson et al., 2012). It thereby provides a direct route for AW from Baffin Bay to enter its inner fjord basins and access over a dozen marine-terminating outlet glaciers which drain this sector of the GrIS (Fig. 1). The existence of two large marine-terminating outlet glaciers, Rink and Store, which drain this sector into Uummannaq Bay, make it a useful target to isolate and compare individual tidewater glacier responses to similar atmospheric and oceanic forcing but with contrasting bed, fjord and frontal geometries and geological controls. Rink and Store glaciers are the second and third largest outlets in west Greenland after Jakobshavn Isbræ, with an estimated discharge of 11–17 $km^3\,year^{-1}$ and 14–18 $km^3\,year^{-1}$ respectively (Weidick and Bennike, 2007). This corresponds to 7 and 8 % of the total annual discharge for the western GrIS (Rignot et al., 2008). A recent aerial study of Store Glacier's terminus calculates the mass flux through the calving front of Store Glacier to be 11.5 $km^3\,year^{-1}$ (Ryan et al., 2014). Both glaciers and fjords are over 5 km wide and at least 100 km long with catchment sizes of 45 000 km^2 for Rink and 34 000 km^2 for Store (Rignot et al., 2008). Despite this, Store has a larger ablation area due to its lower-lying hypsometric profile. Bathymetric mapping reveals that both fjords have an inner basin deeper than 1000 m and that the maximum depth of the calving front of Rink Glacier is ~ 750 m, and at Store Glacier it is ~ 500 m. At Rink Fjord a transverse sill is located 50 km from the ice front with a minimum depth of ~ 400 m (Dowdeswell et al., 2014) whist Store Fjord has no such sill or obstruction to the outer trough (Fig. 1).

3 Methods

3.1 Data collection

Two hydrographic surveys were conducted in August 2009 and 2010 comprising of 5 and 7 conductivity, temperature, turbidity and depth (hereafter called CTD) casts at Rink Fjord and 12 and 11 casts at Store Fjord respectively. The CTD casts were taken along and across each fjord, at a distance of between 200 m and 20 km from their respective calving fronts (Figs. 1 and 2) and to a maximum depth of 750 m. The hydrographic instrument used was a MIDAS Valeport 2000 conductivity–temperature–depth profiler, equipped with a Seapoint turbidity sensor (Table 1). Measurements were logged at a sampling rate of 4 Hz with a descent rate of 1–2 $m\,s^{-1}$, yielding 10 to 20 samples for every 5 m of vertical profile. The instrument also logged on recovery, which at a slower ascent rate of 0.3–0.5 $m\,s^{-1}$ provided ~ 40 samples per 5 m vertical interval. Data were filtered by remov-

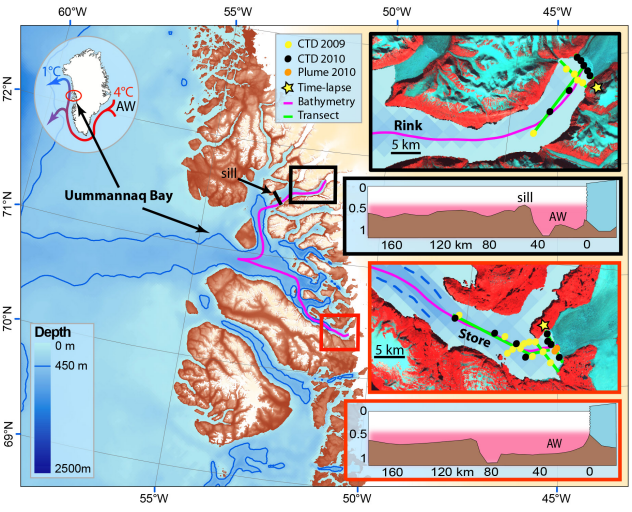

Figure 1. Map of the study area. The yellow and black dots represent the CTD sections in 2009 and 2010 respectively. In the International Bathymetry Chart of the Arctic Ocean (IBCAO), the 450 m contour has been highlighted in blue to indicate the trough across the continental shelf allowing the AW to enter the fjord. Bathymetry of the centre line of Store and Rink fjords are shown for each fjord and correspond approximately to the purple line on the maps. Position of the shallowest sill in Rink Fjord is shown as a thick black line. Orange dots show the position of Store 2010 profiles inside and outside the surface plume. Note that although the IBCAO bathymetry appears to be correct for the outer part of the fjord, that of the inner fjords is inaccurate, as depths of up to 800 and 1100 m are observed near Store and Rink fronts, respectively. A false colour Landsat mosaic from August 2010 is used for the inset maps, superimposed over land and glaciers. Topography (brown shade) and ice mask (off-white) are taken from Greenland Ice Map Project (GIMP).

ing points of more than one standard deviation from the unweighted moving average window ($n = 16$) to yield a statistically significant result. The filtered data were then averaged into 5 m vertical bins. Both the ascent and descent data were used to improve error estimation. The standard deviation provides an indication of measurement uncertainty and corresponds to $\pm 0.023\,^{\circ}\mathrm{C}$ for potential temperature, ± 0.025 PSU for salinity and ± 1.4 nephelometric turbidity unit (NTU) for the turbidity. Potential temperature (θ) and salinity (S) were calculated according to the equations of state of seawater published by UNESCO 1983 (Fofonoff and Millard, 1983) and used to identify specific water bodies and mixing processes.

The turbidity in the fjord was used to trace the sediment-loaded subglacial fresh water (Bartholomew et al., 2011; Motyka et al., 2003). Turbidity estimates are, however, based on backscattering on light, depending of both sediment concentration and type (lithology and size) of particles, which can vary from one fjord to another. To compare the extent of fresh-water-induced buoyant upwelling plumes, we expressed the turbidity as a percentage of the maximum value recorded in each fjord (i.e. within the plumes).

3.2 Water-body identification

When plotted in potential temperature–salinity (θ–S) space, two types of water body can be differentiated: (a) Water types are defined by thick, homogenous layers, in excess of 50 m within the water profile, which share similar temperature and salinity ($\Delta\theta < 0.2\,^{\circ}\mathrm{C}$ and $\Delta S < 0.2$ PSU). Such water types can be identified by dense clustering on a θ–S diagrams; (b) Mixed water masses are defined as a layer within the water column combining two water types and are characterised by the line joining the two water types on the θ–S diagram. We define a mixed water mass when its thickness exceeds 50 m, its $\delta\theta/\delta S$ gradient is constant and when there is sufficient difference ($\Delta\theta > 0.5\,^{\circ}\mathrm{C}$ and/or $\Delta S > 0.5$ PSU) between the top and the bottom of the layer.

3.3 Identification of interaction processes

To isolate which water body is driving subaqueous melt, we calculate the temperature and salinity loss due to the melting of glacier ice with reference to the Gade-slope (Gade, 1979; Holland and Jenkins, 1999; Mortensen et al., 2013; Straneo et al., 2011, 2012). Given a potential temperature for glacier ice (θ_{i}) at the front, we define an effective potential temperature (θ_{eff}) of the corresponding virtual water type by calculating the energy required to melt a unit weight of ice as follows:

$$\theta_{\mathrm{eff}} = \theta_{\mathrm{f}} - \frac{L_{\mathrm{i}} - C_{\mathrm{i}}(\theta_{\mathrm{f}} - \theta_{\mathrm{i}})}{C_{\mathrm{sw}}}, \quad (1)$$

where θ_{f} is the pressure-corrected melting point of ice, L_{i} ($337\,\mathrm{kJ\,kg^{-1}}$) is the latent heat of fusion, C_{i} ($2.1\,\mathrm{kJ\,kg^{-1}\,K^{-1}}$) the specific heat capacity of ice and C_{sw} ($3.9\,\mathrm{kJ\,kg^{-1}\,K^{-1}}$) the specific heat capacity of seawater. In the θ–S diagram, the mixed water mass resulting from submarine melting of the glacier will fall on the Gade-slope joining the water, driving the melt and the virtual water type with characteristics $\theta = \theta_{\mathrm{eff}}$ and $S = 0$. A similar identification procedure can be applied to track runoff mixing and resulting mixed water mass as it will follow a line joining the ambient water and the fresh runoff water ($\theta = 0\,^{\circ}\mathrm{C}$; $S = 0\,^{\circ}\mathrm{C}$) (Mortensen et al., 2013; Straneo et al., 2011, 2012) (hereafter called the runoff slope). If both submarine melting and runoff mixing are affecting the same water parcel, the resulting mixed water mass will have a θ–S gradient proportional to the theoretical slope of each process (Mortensen et al., 2013).

3.4 Interpolation of oceanic measurements

Temperature, salinity and turbidity were interpolated across and along Rink and Store fjords. The cross profile was interpolated immediately adjacent to each ice front (~ 200 m)

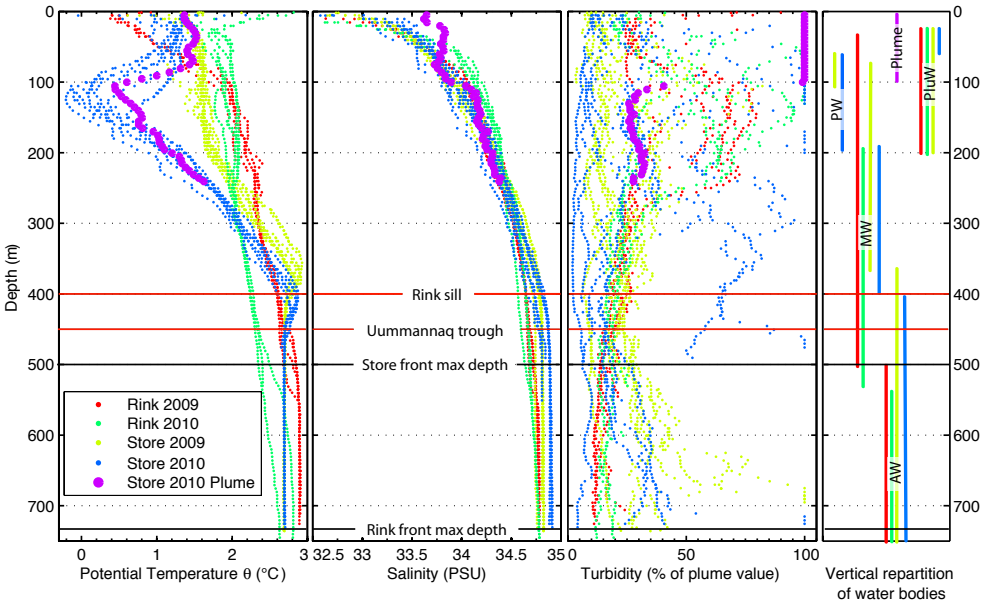

Figure 2. Potential temperature, salinity and turbidity vs. depth for all profiles. On the right-hand side panel, each water-body vertical extent is represented for each survey. The estimated maximal depth of each glacier front is shown with a continuous horizontal black line. The depth of Uummannaq Trough and Rink Sill are shown as horizontal red lines. The turbidity has been converted to a percentage of the maximum value measured inside the plume of each fjord. For Store in 2010, the profile inside the plume (ST 16) is shown in purple.

Table 1. Profiler's sensors (CTD) specifications, MIDAS Valeport 2000.

Sensor	Pressure	Conductivity	Temperature	Turbidity
Type	Strain gauge	Valeport inductive coils	Fast-response platinum thermometer	Seapoint
Accuracy	0.2 Bar	0.01 mS cm^{-1}	0.01 °C	15 NTU

and the long-profile section tracks the midpoint of each fjord (Fig. 1).

3.5 Runoff discharge estimation

In addition to synoptic meteorological conditions, surface glacier meltwater runoff is dependent upon the ablation area, its hypsometry and the seasonal distribution of snow/ice and its concomitant albedo. Monthly mean values of surface melt for each glacier were estimated following Box (2013) using a positive degree-day/melt-rate model applied to glacier catchment. The catchment of each glacier was determined from the GIMP digital elevation model (DEM) of the ice sheet (Bamber et al., 2013). For the purposes of this study we assume an efficient, fully developed drainage system as would be expected in the latter half of the melt season where the bulk of surface meltwater runoff drains and is discharged directly into the fjord as subglacial fresh water (Chandler et al., 2013; Schoof, 2010).

4 Results

4.1 Water types present at the glacier front

Compiled θ–S plots reveal that the distinct water bodies observed within both Rink and Store fjords (Figs. 2 and 3, Table 2) interact with their respective calving fronts (Sect. 4.2). Except for polar water (PW) described below, all the other water bodies observed were directly adjacent ($\sim$ 200 m) to each glacier and can be assumed to be in direct contact with the submerged calving face. Four distinct water types were observed:

1. Surface water (SW) is the uppermost layer of the fjord and is strongly affected by solar insolation, atmospheric forcing, brash-ice melt as well other external processes including river runoff and vertical mixing (Mortensen et al., 2011). In this study, the pycnocline at the lower interface of the SW appears to act as a barrier to buoyant upwelling waters (Sect. 4.4) often constraining them below the SW. Throughout our surveys, SW was limited to the upper 15 m of the water column with temperatures ranging from 0 to 10 °C and in salinity from 28

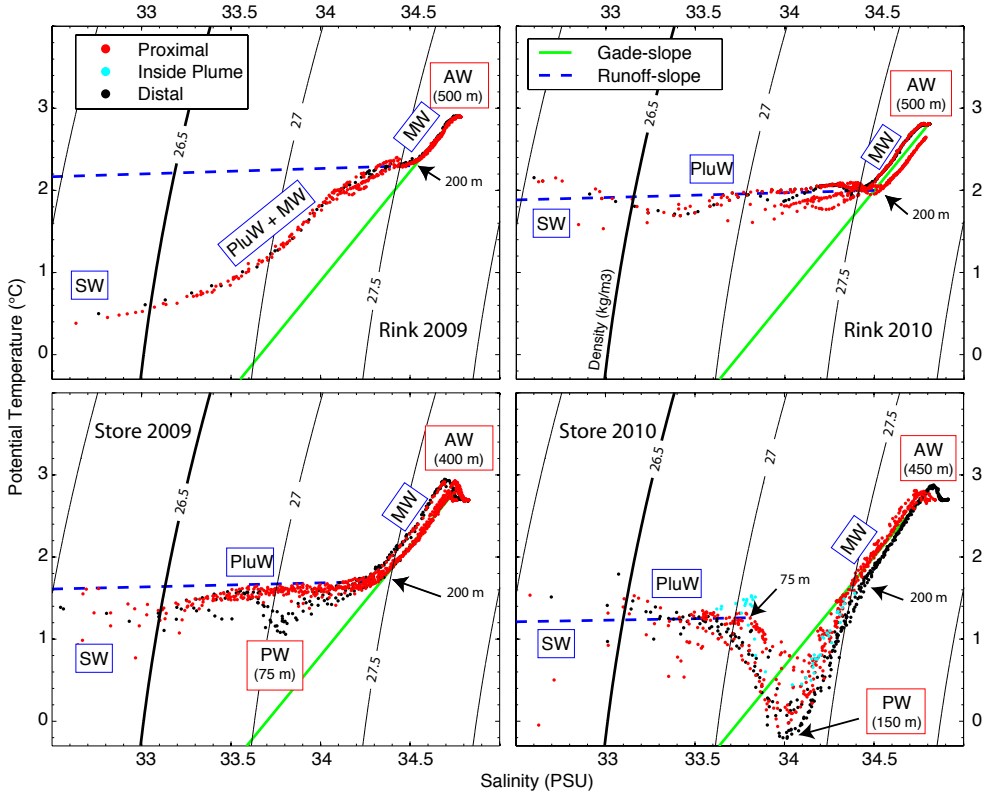

Figure 3. Potential temperature–salinity diagram of the CTD stations in 2009 and 2010 for Rink and Store fjords. The distal (∼ 20–30 km) and proximal (∼ 0.2–1 km) profiles are in black and red, respectively. The labels and the depth of the water types are outlined in red whilst the mixed water masses are in blue. Isopycnals are in black with $\sigma = 26.5\,\mathrm{kg\,m^{-3}}$ highlighted in bold to represent the lower limit of the surface water. Green continuous and blue dashed lines represent the theoretical Gade-slope and runoff slope, respectively.

to 33 PSU. We define the limit of the SW by its density ($\sigma_\theta < 26.5\,\mathrm{kg\,m^{-3}}$) as it is above this value that most of the variability appears.

2. Atlantic water (AW) (Straneo et al., 2012), also known as subpolar mode water (Mortensen et al., 2011) or intermediate Irminger water (Ribergaard, 2007), is the deepest and warmest water body present in the fjord. This water type is advected along the coast by the west Greenland Current (Mortensen et al., 2011, 2013; Ribergaard, 2007; Straneo and Heimbach, 2013; Straneo et al., 2012), entering the fjord via the Uummannaq Bay trough carved across the continental shelf. Throughout our surveys, AW was always present below 400 to 500 m depth and had highly consistent temperature and salinity characteristics ($\theta = 2.8 \pm 0.2\,^\circ\mathrm{C}$ and $S = 34.8 \pm 0.1$ PSU) for both fjords over both years.

3. Polar water (PW), which was only observed in Store Fjord, is the coldest water body (Figs. 2 and 3). PW originates from the Arctic Ocean (Hopkins, 1991) and is present along the west coast of Greenland at 50 to 150 m depth (Ribergaard, 2007) where it would be able to advect into Uummannaq Bay. In 2010 at Store, PW was observed at 50 to 200 m depth, separating SW and AW, and had a minimum temperature of $\theta \sim= 0\,^\circ\mathrm{C}$ and $S = 34$ PSU at ~ 150 m. Remnant traces of PW were visible at Store in 2009 for the most distal CTD cast (~ 10 km from the glacier) but were not observed any nearer or in direct contact with the calving front (Fig. 4). PW was not observed in Rink Fjord in either year.

4. Subglacial fresh water (SgFW) includes basal as well as surface runoff and is injected into the fjords at distinct portals at depth in the calving front. SgFW is very difficult to measure in its original state due to the vigorous mixing which occurs on its injection from the portal (Salcedo-Castro et al., 2011; Xu et al., 2012, 2013). Hence, SgFW is reasonably assumed to have the basic characteristics of $\theta = 0\,^\circ\mathrm{C}$ and $S = 0$ PSU (Mortensen et al., 2013; Straneo et al., 2012).

4.2 Mixed water masses and inferred processes

4.2.1 Submarine melting

Applying Eq. (1) and assuming a temperature for glacier ice of $\theta_\mathrm{i} = -10\,^\circ\mathrm{C}$ (taken from Jakobshavn Isbræ; Thomas,

Table 2. Characteristics of the water types and mixed waters observed during the surveys.

	Water types			Mixed water masses		
	AW	PW	SgFW	MW	PluW	SW
[θ(°C);S(PSU)] or [δ(°C)/δS(PSU)]	[2.8; 34.8]	[0; 34]	[0; 0]	(2.5)	(0.05)	NA
Origin	Subpolar gyre	Arctic Ocean	Surface/basal glacier melt	Resulting from submarine melting	Resulting from runoff mixing	River mixing, solar insolation
Transport	Advected by WGC	Advected by WGC	Local formation	Local formation	Local formation	Local formation
Depth range	400 m bottom	∼ 50–200 m	∼ 500 m (Store) ∼ 750 m (Rink)	200– ∼ 400 m	15–200 m or 15–75 m	0–15 m

2004) and a salinity (S_i) of 0 PSU at the base of Store calving front yields a virtual water-type temperature of $\theta_{eff} = -89.8$ °C. Note that θ_{eff} is not sensitive to the assumed values of θ_i. Hence, meltwater (MW) driven by AW ($S = 34.8$ PSU and $\theta = 2.8$ °C) will follow a Gade-slope of ~ 2.7 °C PSU^{-1}. MW was found in all surveys above the AW and below SW (or PW if present). The gradient derived from our observations of MW of ~ 2.5 °C PSU^{-1} is in good agreement with the theoretical Gade-slope (Fig. 3). MW was observed from 100 to 250 m from the base of the calving front up to 200 m from the surface (Fig. 2). Rink Fjord in 2009 was an exception when MW was present along with plume water (see below) from 200 m to 15 m depth (Fig. 3). The presence of MW below the outer sill depth at Rink Fjord (Fig. 2) indicates that it is formed locally by interaction with the calving front and is not merely advected in from Baffin Bay.

4.2.2 Runoff mixing

Following Straneo et al. (2011, 2012), the horizontal inflection in the θ–S diagram is used to define the second apex of the runoff slope (Fig. 3) and gives a theoretical value of ~ 0.05 °C PSU^{-1} and 0.04 °C PSU^{-1} respectively. Plume water (PluW) is produced by the mixing of SgFW with ambient fjord water at depth and is sometimes referred to as subglacial water (Mortensen et al., 2011). In our surveys, PluW has a runoff slope of ~ 0.07 °C PSU^{-1} (Fig. 3) and was found below the SW and above a depth of either 200 m (Rink 2009–2010 and Store 2009) or 75 m (Store 2010) depth.

Mixing of MW and PluW with similar proportions to each other was only observed in 2009 at Rink within the upper layer.

Due to the lack of direct observation of plume processes (within tens of metres of the ice front), the inflection in the θ–S diagram (Fig. 3) reflects the depth at which the PluW outflows horizontally and not the depth of injection of the SgFW into the fjord.

4.3 SgFW discharge estimation

The surveys were conducted in August of 2009 and 2010 during two contrasting melt seasons with very different glacier meltwater runoff characteristics. In 2009, air temperatures and glacial melt were normal and approximate the 2000 to 2010 mean, whereas temperature, extent and magnitude of surface melt were record-setting in 2010 (Tedesco et al., 2011; van As et al., 2012). In the absence of precipitation during both sets of surveys we assume that the monthly variations in the discharge of SgFW are predominantly driven by glacier surface melt. Surface melt runoff modelling yields a predicted SgFW discharge at Rink of 1000 ± 300 m^3 s^{-1} in 2009 and 1500 ± 450 m^3 s^{-1} in 2010. At Store, the SgFW discharge is estimated at 1500 ± 450 m^3 s^{-1} in 2009 and 2000 ± 600 m^3 s^{-1} in 2010. Uncertainties are defined by the 30 % standard error derived from comparisons between modelled (Box, 2013) and measured (van de Wal et al., 2012) runoff at the Kangerlussuaq transect, some 300 km to the south of our study site. Given that Rink and Store catchments are within the same fjord system, it can be noted that any bias in the runoff model should affect both glaciers consistently and hence the relative variation in discharge of SgFW for the two glaciers can be compared directly. The SgFW discharge of Store Glacier in 2009 was ∼ 50 % greater than that for Rink, due to the latter's reduced ablation area. Driven by very high air temperatures in August 2010, SgFW discharge at both glaciers is amplified by ∼ 50 % compared to 2009.

4.4 Turbidity analysis and plume observation

At Store, a variable turbid plume was visible at the water surface adjacent to the calving front in time-lapse imagery acquired in July 2009 (http://vimeo.com/2638166) (Ahn and Box, 2010), but was not visible in August. In contrast, in August 2010, a large, dominant turbid plume extended ∼ 1 km away from the ice front. Logging of the time-lapse imagery indicates that the forced convection associated with

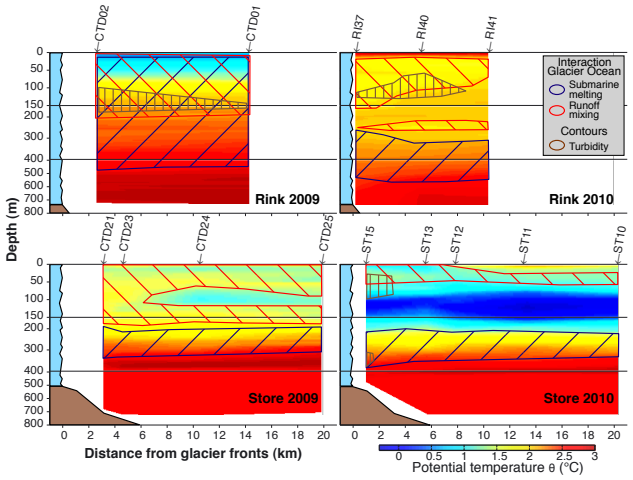

Figure 4. Potential temperature along fjord section (parallel to the fjord main axis), with the glacier front to the left and the open ocean to the right. Dashed areas show waters resulting from submarine melting (blue) and runoff mixing (red). The brown dashed area corresponds to a turbidity > 80 % of the maximum recorded in the plume. The estimated bottom profile is depicted as a solid brown area.

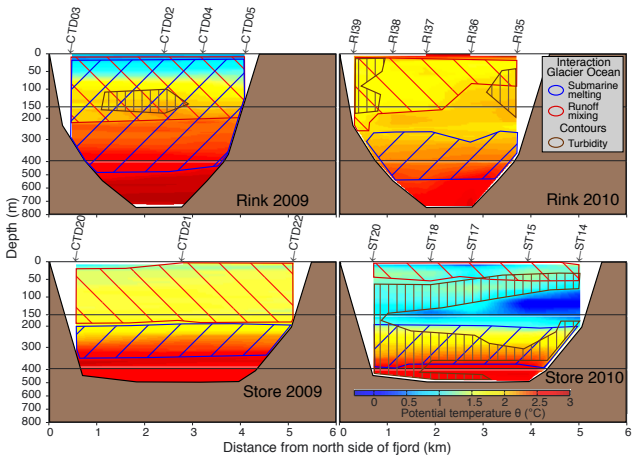

Figure 5. Same as Fig. 4, but with the across-fjord section (parallel to the front at ∼ 200–1000 m distance). The north side of the fjord is on the left and it is facing the ice front.

the plume was attaining the surface from June until the end of August 2010. Horizontal surface outflow from this plume attained speeds up to $\sim 1.5\,\mathrm{m\,s^{-1}}$, sufficient to force brash ice or mélange out from the embayment (Fig. 8). A distinct boundary was observed at the outer limit of the plume, visible by a marked change in water turbidity (Fig. 8). The outflow of PluW is observed at 50–100 m depth (Fig. 5) and extends up to 3 km away from the front (Fig. 4). A layer of intense turbidity was also observed from 300 m depth to the bottom (Figs. 4, 5 and 7) at Store in 2010 (Fig. 5). Turbidity measurements within and just outside of the surface plume (visually defined by the contrast in water colour), indicate that PluW sinks below the pycnocline of the SW after attaining the surface (Fig. 7), an observation that is in agreement with plume modelling at Store (Xu et al., 2013).

In contrast to Store, there was very little surface plume activity observed at Rink. Logging of time-lapse photography of Rink (http://vimeo.com/6038577) (Ahn and Box, 2010) reveals just one surface plume on its southern margin in July 2009 and 2010, which had, however, disappeared completely by early August. Despite this apparent absence of surface plume activity, turbid waters were observed just below SW, suggesting that the plume was still present but was not attaining the surface. In August 2009, a submarine turbid water jet was present in the middle of the cross section between 100 and 200 m depth and spreading up to 10 km down the fjord (Fig. 4). In August 2010, two turbid jets are present, one along the north side of the fjord and one along the south side with the strongest jet measured beneath the pycnocline of the SW at 15 m depth (Fig. 5).

5 Discussion

5.1 Ocean–glacier interaction

The hydrographic surveys at Rink and Store provide four snapshots of glacier–ocean interaction during the latter half of the melt season when SgFW discharge should be most pronounced. Direct observation of these interactions and their repartitioning within the water column shows marked similarities and differences between both years and the fjords from which we identify key suites of processes significantly and simultaneously impacting a water parcel (hereafter called states). Below 200 m depth, free convective submarine melting is the only process which is consistently identified (Figs. 4 and 5), whereas three different states can be distinguished within the upper layers of the water column (0–200 m depth): state (1) – submarine melting interlaced with runoff mixing both of similar magnitude (Rink 2009); state (2) – significant runoff mixing (Store 2009 and Rink 2010); state (3) – similar to state 2 but with a shallower (< 75 m depth) outflow (Store 2010).

Comparison of these observed states with calculated SgFW discharge suggests that the interaction processes in the upper layer are potentially influenced by glacier meltwater runoff rates. Indeed, when the SgFW discharge increases at Store, the PluW outflow becomes shallower and evolves from state 2 to state 3 (Fig. 6), an observation which resonates with recent modelling (Sciascia et al., 2013; Xu et al., 2013).

At Rink, in 2009, both PluW and MW were observed in similar proportions in the upper layer. By contrast, in 2010 PluW was the only water to contribute significantly to the upper layer. As both the temperature and depth of the AW as well as the vertical extent of submarine melting remained the same in the 2009 and 2010 surveys, we infer that the 50 %

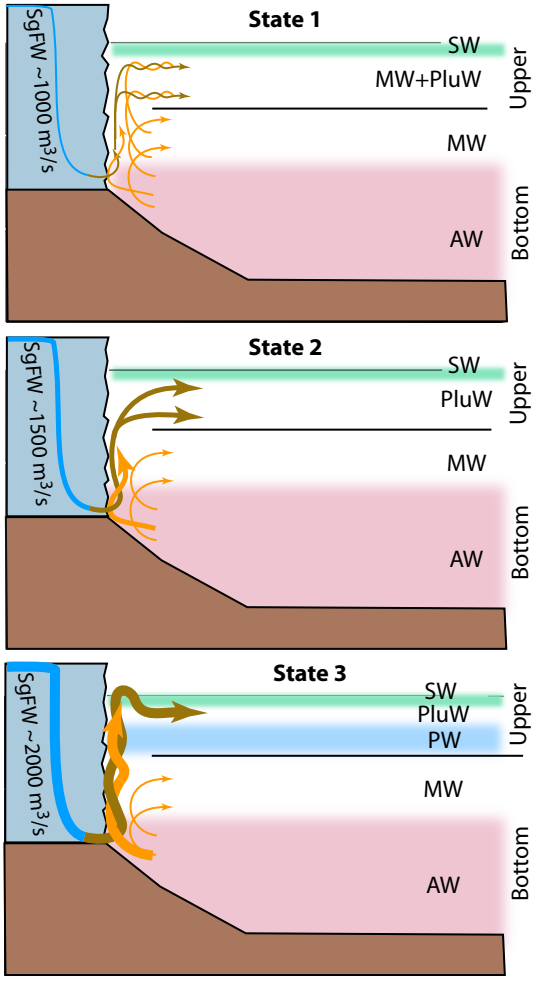

Figure 6. Simplified schematic of the three states of interaction identified (Sect. 5.1), the associated SgFW discharge and the circulation induced at the glacier front. The arrow thicknesses represent an approximate magnitude, and the colours represent the different processes of interaction with the following: SgFW (blue), runoff mixing (brown) and submarine melting (orange). The upper and bottom layers are represented above and below 200 m depth. Each water body observed in the water column is labelled as in the text (Sects. 4.1 and 4.2)

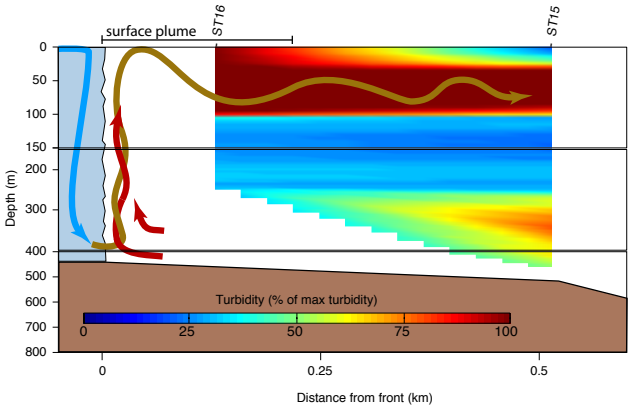

Figure 7. Turbidity section across the boundary of the surface plume at Store in 2010 (Fig. 8). The turbidity is shown as a percentage of the maximum turbidity recorded in the plume. The profile ST15 was done ∼ 200 m outside the turbid plume where the surface of the sea was a normal blue colour and no significant surface current was observed. The profile ST16 was done ∼ 100 m inside the surface plume, the colour of the surface was dark brown and a strong turbulent current flowing away from the glacier was observed. ST16 was not lowered to the bottom of the fjord for safety reasons, therefore interpolation below 250 m is not realistic. The arrows show a schematics circulation in the plume with SgFW in blue, AW in red and PluW in brown.

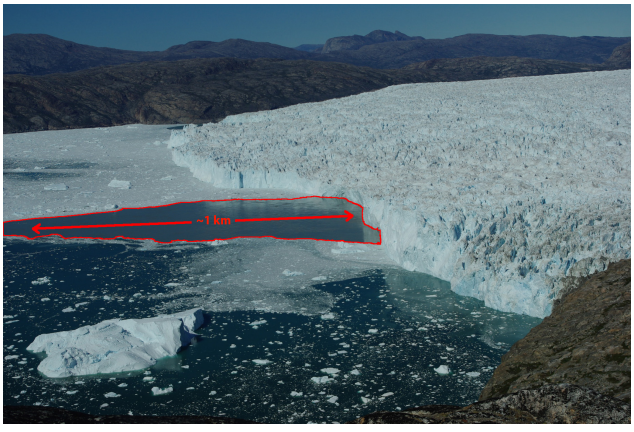

Figure 8. Picture taken from the southern side of Store Glacier in 2012 (looking north). The red line shows the boundary of the turbid surface plume observed from June to September and its approximate extent.

stronger SgFW discharge in 2010 is responsible for a more pronounced runoff-mixing impact and hence PluW contribution.

A simplified schematic of the three observed states of ocean–glacier interaction and the associated circulation patterns are presented (Fig. 6). Excluded from this schematic are external factors such as wind-driven circulation (Straneo et al., 2010; Sutherland and Straneo, 2012), tides (Mortensen et al., 2011) and seasonality of the forcing cycle (Mortensen et al., 2013), all of which will influence the circulation patterns as well.

Despite these limitations, the circulation induced by the runoff mixing and submarine melting, and its evolution, must significantly contribute to the general circulation across and along the glacier front. Indeed, both processes produce vertical entrainment of ambient AW water in direct contact with the ice front, which is a major driver of enhanced melting at the calving front (Jenkins, 1991, 2011; Josberger and Martin, 1981; Xu et al., 2012, 2013).

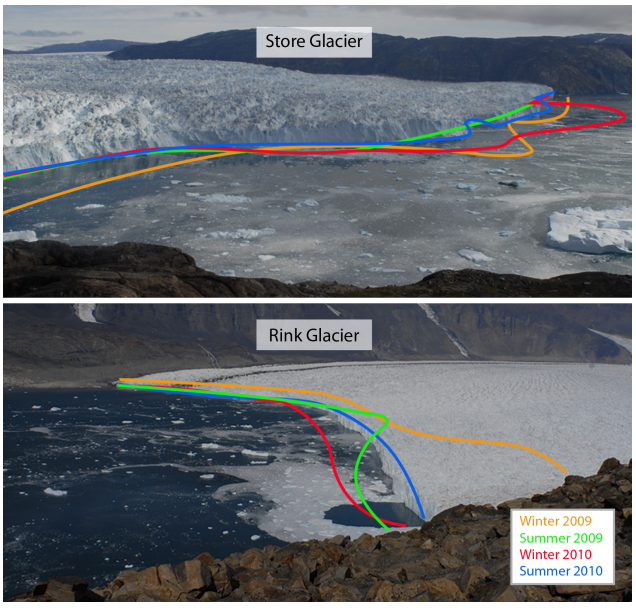

Figure 9. Time-lapse photographs of Store and Rink glacier termini in August 2010. The general shape and position of each glacier front for the winter preceding each survey and the summer of the survey have been outlined in orange (winter 2009), green (summer 2009), red (winter 2010) and blue (summer 2010).

5.2 SgFW-driven upwelling: spatial spreading and glacier impact

Glacier buoyant upwelling plumes, producing PluW, are commonly associated with enhanced submarine melting through the entrainment of warm water along the ice front (Jenkins, 2011; Motyka et al., 2003, 2011; Rignot et al., 2010; Sciascia et al., 2013; Sole et al., 2012; Xu et al., 2012, 2013). The scale of the subglacial channels allowing SgFW to enter the fjord is, to date, not well defined (Jenkins, 2011; Sciascia et al., 2013; Xu et al., 2013). It has been hypothesised that emerging SgFW is channelised and hence injected through discrete portals (Jenkins, 2011; Mugford and Dowdeswell, 2011) rather than being evenly injected all along the front (Sciascia et al., 2013; Sole et al., 2012; Xu et al., 2012; 2013). This is in agreement with the well-defined surface plume observed at Store (Fig. 8) and elsewhere (Mortensen et al., 2013; Motyka et al., 2003; Rignot et al., 2010; Xu et al., 2013), which indicates a point source injection at depth, and with the presence of turbid jets at Rink (Fig. 5) which also have a distinct spatial footprint. In all surveys, the layer of PluW was, nevertheless, present uniformly across the fjord near the glacier and fading downstream (Figs. 4 and 5), suggesting that despite the potential localised injection point, PluW rapidly spreads across as well as along the fjord at its depth of hydrostatic equilibrium.

5.3 Oceanic and bathymetric influence on glacier front behaviour

The presence of sills in Uummannaq Bay has a strong impact on how water is transported into the deeper fjords and toward each of the glaciers' calving fronts. The trough on the continental shelf near Uummannaq entrance provides access for all water above 450 m to penetrate as far as Store. At Rink, the presence of an additional sill at 400 m depth and 50 km down the fjord (Dowdeswell et al., 2014) further affects the temperature of water found at Rink's calving front. Indeed, we found the bottom water at Rink to have the characteristics of the AW found at Store at 400 m depth (i.e. the depth of Rink sill) (Fig. 2).

At Rink Glacier, mass loss (i.e. calving and submarine melt combined), logged by time-lapse photography, appears to be relatively homogeneous across the entire ice front with maximum losses at the central sector, coincident with the deepest part of the fjord and fastest ice flow. At Store Glacier, frontal mass loss during both summers is greater on the southern flank, where a large embayment between two headlands coincides with an upwelling plume visible at the surface. These observations suggest that in addition to the fjord geometrical control on the glacier calving processes (McFadden et al., 2011; Schild and Hamilton, 2013), the presence of warm, subpolar-originating water bodies at the glacier front, along with the presence of sills and inner basins in the fjord, also has a considerable impact on the calving dynamics, and thus on the shape of the calving front. We hypothesise that deep tidewater glaciers, such as Rink (~ 750 m), which are exposed significantly to warm AW at their base (~ 75 % at Rink), will be influenced by widespread, submarine melting, which would favour a relatively flat calving face (Fig. 9). For glaciers such as Store, which have a shallower ice front (< 500 m), the impact of SgFW discharge on the upper layer (0–200 m) may be the primary factor driving frontal geometry and dynamics. We suggest that notch cutting and the resulting headlands along the ice front are related to the presence of localised plume-induced melting of the ice front where SgFW is released from subglacial portals (Figs. 8 and 9). The local undercutting of the calving face will, in this case, create a crenulated ice front characterised by a series of embayments and separated by headlands where calving processes will dominate.

6 Conclusions

Hydrographic surveys in Uummannaq Bay in August 2009 and 2010 reveal that warm ($2.8 \pm 0.2\,^{\circ}$C) and deep Atlantic water (AW) was present below 450 m and driving free convective submarine melting of Rink and Store, two fast-flowing outlets of west Greenland. Subglacial fresh water (SgFW) injected at depth was also observed to force buoyant plumes where runoff mixing is the main process involved,

yielding a turbid outflow of plume water (PluW). Turbidity transects across the upwelling plumes show that, after attaining the surface, the plume sinks below surface water (SW) and replaces any water present at its level of outflow along and across the fjord. The plumes do not necessarily surface in the fjords, as revealed by jets of turbid water, observed at depths of 50 to 100 m. Two layers can be distinguished in the fjord structure. The upper layer (0–200 m) experiences the greatest differences in between the fjords and surveys, with three different states of interaction observed: submarine melting and runoff mixing (state 1), runoff mixing alone (state 2) and runoff mixing alone at shallower depth (75 m) (state 3). The evolution of the upper layer structure from state 1 to state 3 is hypothesised to be primarily controlled by the increase of SgFW discharge. The bottom layer below 200 m depth has similar characteristics in all surveys, with free convective submarine melting being the only process involved. At Rink Glacier, which is 750 m deep, $\sim$ 75 % of the ice front is affected by submarine melting which favours a relatively flat calving front. In contrast, at Store, which is up to 500 m deep, SgFW discharge and buoyancy-driven plumes affect over 40 % of the calving front, leading to a crenulated terminus characterised by a series of notches separated by headlands which are exposed to mechanical failure and calving.

Acknowledgements. We wish to acknowledge fieldwork support from NERC Grant NE/G010595/1, the Aberystwyth University Research Fund and the Royal Geographical Society. N. Chauché is supported by an Aberystwyth University Research Studentship and wishes to acknowledge the support of LOCEAN (University of Pierre and Marie Curie, UPMC). J. E. Box was supported by The Ohio State University's Climate Water and Carbon initiative managed by D. Alsdorf and the Geological Survey of Denmark and Greenland. J.-C. Gascard acknowledges the support of Arctic Climate Change, Economy and Society (ACCESS). We are indebted to the tireless crew of S/V *Gambo* and all those who have supported this project, particularly the Uummannaq Polar Institute and Children's Home.

Edited by: E. Larour

References

Ahn, Y. and Box, J. E.: Glacier velocities from time-lapse photos: technique development and first results from the Extreme Ice Survey (EIS) in Greenland, J. Glaciol., 56, 723–734, 2010.

Bamber, J. L., Griggs, J. A., Hurkmans, R. T. W. L., Dowdeswell, J. A., Gogineni, S. P., Howat, I., Mouginot, J., Paden, J., Palmer, S., Rignot, E., and Steinhage, D.: A new bed elevation dataset for Greenland, The Cryosphere, 7, 499–510, doi:10.5194/tc-7-499-2013, 2013.

Bartholomew, I., Nienow, P., Sole, A., Mair, D., Cowton, T., Palmer, S., and Wadham, J.: Supraglacial forcing of subglacial drainage in the ablation zone of the Greenland ice sheet, Geophys. Res. Lett., 38, doi:10.1029/2011GL047063, 2011.

Box, J. E.: Greenland Ice Sheet Mass Balance Reconstruction. Part II: Surface Mass Balance (1840–2010), J. Climate, 26, 6974–6989, doi:10.1175/JCLI-D-12-00518.1, 2013.

Chandler, D. M., Wadham, J. L., Lis, G. P., Cowton, T., Sole, A., Bartholomew, I., Telling, J., Nienow, P., Bagshaw, E. B., Mair, D., Vinen, S., and Hubbard, A.: Evolution of the subglacial drainage system beneath the Greenland Ice Sheet revealed by tracers, Nat. Geosci., 6, 195–198, doi:10.1038/ngeo1737, 2013.

Christoffersen, P., O'Leary, M., Van Angelen, J. H., and van den Broeke, M.: Partitioning effects from ocean and atmosphere on the calving stability of Kangerdlugssuaq Glacier, East Greenland, Ann. Glaciol., 53, 249–256, doi:10.3189/2012AoG60A087, 2012.

Dowdeswell, J. A., Hogan, K. A., Ó Cofaigh, C., Fugelli, E. M. G., Evans, J., and Noormets, R.: Late Quaternary ice flow in a West Greenland fjord and cross-shelf trough system: submarine landforms from Rink Isbrae to Uummannaq shelf and slope, Quaternary Sci. Rev., 92, 292–309, doi:10.1016/j.quascirev.2013.09.007, 2014.

Fofonoff, N. and Millard, R. C.: Algorithms for Computation of Fundamental Properties of Seawater. Endorsed by Unesco/SCOR/ICES/IAPSO Joint Panel on Oceanographic Tables and Standards and SCOR Working Group 51. Unesco Technical Papers in Marine Science, No. 44., 1983.

Gade, H. G.: Melting of ice in sea water: A primitive model with application to the Antarctic ice shelf and icebergs, J. Phys. Oceanogr., 9, 189–198, 1979.

Hanna, E., Huybrechts, P., Steffen, K., Cappelen, J., Huff, R., Shuman, C., Irvine-Fynn, T., Wise, S., and Griffiths, M.: Increased Runoff from Melt from the Greenland Ice Sheet: A Response to Global Warming, J. Climate, 21, 331–341, doi:10.1175/2007JCLI1964.1, 2014.

Holland, D. M. and Jenkins, A.: Modeling thermodynamic ice-ocean interactions at the base of an ice shelf, J. Phys. Oceanogr., 29, 1787–1800, 1999.

Holland, D. M., Thomas, R. H., de Young, B., Ribergaard, M. H., and Lyberth, B.: Acceleration of Jakobshavn Isbrae triggered by warm subsurface ocean waters, Nat. Geosci., 1, 659–664, 2008.

Hopkins, T. S.: The GIN Sea – A synthesis of its physical oceanography and literature review 1972–1985, Earth-Sci. Rev., 30, 175–318, 1991.

Hubbard, A. L.: The Times Atlas and actual Greenland ice loss, Geology Today, 27, 212–215, doi:10.1111/j.1365-2451.2011.00812.x, 2011.

Jakobsson, M., Mayer, L., Coakley, B., Dowdeswell, J. A., Forbes, S., Fridman, B., Hodnesdal, H., Noormets, R., Pedersen, R., Rebesco, M., Schenke, H. W., Zarayskaya, Y., Accettella, D., Armstrong, A., Anderson, R. M., Bienhoff, P., Camerlenghi, A., Church, I., Edwards, M., Gardner, J. V., Hall, J. K., Hell, B., Hestvik, O., Kristoffersen, Y., Marcussen, C., Mohammad, R., Mosher, D., Nghiem, S. V., Pedrosa, M. T., Travaglini, P. G., and Weatherall, P.: The International Bathymetric Chart of the Arctic Ocean (IBCAO) Version 3.0, Geophys. Res. Lett., 39, L12609, doi:10.1029/2012GL052219, 2012.

Jenkins, A.: A one-dimensional model of ice shelf-ocean interaction, J. Geophys. Res., 96, 20671–20677, 1991.

Jenkins, A.: Convection-Driven Melting near the Grounding Lines of Ice Shelves and Tidewater Glaciers, J. Phys. Oceanogr., 41, 2279–2294, doi:10.1175/JPO-D-11-03.1, 2011.

Josberger, E. G. and Martin, S.: A laboratory and theoretical study of the boundary layer adjacent to a vertical melting ice wall in salt water, Journal of Fluid Mechanics, 111, 439–473, 1981.

Joughin, I., Smith, B. E., Howat, I. M., Floricioiu, D., Alley, R. B., Truffer, M., and Fahnestock, M.: Seasonal to decadal scale variations in the surface velocity of Jakobshavn Isbrae, Greenland: Observation and model-based analysis, J. Geophys. Res., 117, F02030, doi:10.1029/2011JF002110, 2012.

Kjær, K. H., Khan, S. A., Korsgaard, N. J., Wahr, J., Bamber, J. L., Hurkmans, R., van den Broeke, M., Timm, L. H., Kjeldsen, K. K., and Bjørk, A. A.: Aerial Photographs Reveal Late–20th-Century Dynamic Ice Loss in Northwestern Greenland, Science, 337, 569–573, 2012.

McFadden, E. M., Howat, I. M., Joughin, I., Smith, B. E., and Ahn, Y.: Changes in the dynamics of marine terminating outlet glaciers in west Greenland (2000–2009), J. Geophys. Res., 116, F02022, doi:10.1029/2010JF001757, 2011.

Mortensen, J., Lennert, K., and Bendtsen, J.: Heat sources for glacial melt in a sub-Arctic fjord (Godthåbsfjord) in contact with the Greenland Ice Sheet, J. Geophys. Res., 116, C01013, doi:10.1029/2010JC006528, 2011.

Mortensen, J., Bendtsen, J., Motyka, R. J., Lennert, K., Truffer, M., Fahnestock, M., and Rysgaard, S.: On the seasonal freshwater stratification in the proximity of fast-flowing tidewater outlet glaciers in a sub-Arctic sill fjord, J. Geophys. Res-Oceans, 118, 1382–1395, doi:10.1002/jgrc.20134, 2013.

Motyka, R. J., Hunter, L., Echelmeyer, K. A., and Connor, C.: Submarine melting at the terminus of a temperate tidewater glacier, LeConte Glacier, Alaska, USA, Ann. Glaciol., 36, 57–65, 2003.

Motyka, R. J., Truffer, M., Fahnestock, M., Mortensen, J., Rysgaard, S., and Howat, I. M.: Submarine melting of the 1985 Jakobshavn Isbræ floating tongue and the triggering of the current retreat, J. Geophys. Res., 116, F01007, doi:10.1029/2009JF001632, 2011.

Mugford, R. and Dowdeswell, J. A.: Modeling glacial meltwater plume dynamics and sedimentation in high-latitude fjords, J. Geophys. Res., 116, F01023, doi:10.1029/2010JF001735, 2011.

Pfeffer, W. T.: A simple mechanism for irreversible tidewater glacier retreat, J. Geophys. Res., 112, F03S25, doi:10.1029/2006JF000590, 2007.

Ribergaard, M. H.: Oceanographic Investigations off West Greenland, Danish Metrological Institute Centre for Ocean and Ice (DMI), Copenhagen, 2007.

Rignot, E., Box, J. E., and Hanna, E.: Mass balance of the Greenland ice sheet form 1958 to 2007, Geophys. Res. Lett., 1–5, L20502, doi:10.1029/2008GL035417, 2008.

Rignot, E., Koppes, M., and Velicogna, I.: Rapid submarine melting of the calving faces of West Greenland glaciers, Nat. Geosci., 3, 187–191, 2010.

Ryan, J. C., Hubbard, A. L., Todd, J., Carr, J. R., Box, J. E., Christoffersen, P., Holt, T. O., and Snooke, N.: Repeat UAV photogrammetry to assess calving front dynamics at a large outlet glacier draining the Greenland Ice Sheet, The Cryosphere Discuss., 8, 2243–2275, doi:10.5194/tcd-8-2243-2014, 2014.

Salcedo-Castro, J., Bourgault, D., and deYoung, B.: Circulation induced by subglacial discharge in glacial fjords: Results from idealized numerical simulations, Cont. Shelf Res., 31, 1396–1406, 2011.

Schild, K. M. and Hamilton, G. S.: Seasonal variations of outlet glacier terminus position in Greenland, J. Glaciol., 59, 759–770, doi:10.3189/2013JoG12J238, 2013.

Schoof, C.: Ice-sheet acceleration driven by melt supply variability, Nature, 468, 803–806, doi:10.1038/nature09618, 2010.

Sciascia, R., Straneo, F., Cenedese, C., and Heimbach, P.: Seasonal variability of submarine melt rate and circulation in an East Greenland fjord, J. Geophys. Res. Oceans, 118, 2492–2506, doi:10.1002/jgrc.20142, 2013.

Sole, A. J., Payne, A. J., Nienow, P. W., Christoffersen, P., Cottier, F. R., and Inall, M. E.: Increased glacier runoff enhances the penetration of warm Atlantic water into a large Greenland fjord, The Cryosphere Discuss., 6, 4861–4896, doi:10.5194/tcd-6-4861-2012, 2012.

Straneo, F. and Heimbach, P.: North Atlantic warming and the retreat of Greenland's outlet glaciers, Nature, 504, 36–43, doi:10.1038/nature12854, 2013.

Straneo, F., Hamilton, G. S., Sutherland, D. A., Stearns, L. A., Davidson, F., Hammill, M. O., Stenson, G. B., and Rosing-Asvid, A.: Rapid circulation of warm subtropical waters in a major glacial fjord in East Greenland, Nat. Geosci., 3, 182–186, 2010.

Straneo, F., Curry, R., Sutherland, D. A., Hamilton, G. S., Cenedese, C., Våge, K., and Stearns, L. A.: Impact of ocean stratification on submarine melting of a major Greenland outlet glacier, Nature Precedings, 2011.

Straneo, F., Sutherland, D. A., Holland, D. M., Gladish, C., Hamilton, G. S., Johnson, H. L., Rignot, E., Xu, Y., and Koppes, M.: Characteristics of ocean waters reaching Greenland's glaciers, Ann. Glaciol., 53, 202–210, doi:10.3189/2012AoG60A059, 2012.

Sutherland, D. A. and Straneo, F.: Estimating ocean heat transports and submarine melt rates in Sermilik Fjord, Greenland, using lowered acoustic Doppler current profiler (LADCP) velocity profiles, Ann. Glaciology, 53, 50–58, doi:10.3189/2012AoG60A050, 2012.

Sutherland, D. A., Straneo, F., Stenson, G. B., Davidson, F. J. M., Hammill, M. O., and Rosing-Asvid, A.: Atlantic water variability on the SE Greenland continental shelf and its relationship to SST and bathymetry, J. Geophys. Res.-Oceans, 118, 847–855, doi:10.1029/2012JC008354, 2013.

Tedesco, M., Fettweis, X., van den Broeke, M., van de Wal, R. S. W., Smeets, C. J. P. P., van de Berg, W. J., Serreze, M. C., and Box, J. E.: The role of albedo and accumulation in the 2010 melting record in Greenland, Environ. Res. Lett., 6, 014005, doi:10.1088/1748-9326/6/1/014005, 2011.

Thomas, R. H.: Force-perturbation analysis of recent thinning and acceleration of Jakobshavn Isbrae, Greenland, J. Glaciol., 50, 57–66, 2004.

van As, D., Hubbard, A. L., Hasholt, B., Mikkelsen, A. B., van den Broeke, M. R., and Fausto, R. S.: Large surface meltwater discharge from the Kangerlussuaq sector of the Greenland ice sheet during the record-warm year 2010 explained by detailed energy balance observations, The Cryosphere, 6, 199–209, doi:10.5194/tc-6-199-2012, 2012.

van de Wal, R. S. W., Boot, W., Smeets, C. J. P. P., Snellen, H., van den Broeke, M. R., and Oerlemans, J.: Twenty-one years of mass balance observations along the K-transect, West Greenland, Earth Syst. Sci. Data, 4, 31–35, doi:10.5194/essd-4-31-2012, 2012.

Weidick, A. and Bennike, O.: Quaternary glaciation history and glaciology of Jakobshavn Isbræ and the Disko Bugt region, West Greenland: a review, Geological Survey of Denmark and Greenland, 2007.

Xu, Y., Rignot, E., Fenty, I., Menemenlis, D., and Flexas, M. M.: Subaqueous melting of Store Glacier, west Greenland from three-dimensional, high-resolution numerical modeling and ocean observations, Geophys. Res. Lett., 40, 4648–4653, doi:10.1002/grl.50825, 2013.

Xu, Y., Rignot, E., Menemenlis, D., and Koppes, M.: Numerical experiments on subaqueous melting of Greenland tidewater glaciers in response to ocean warming and enhanced subglacial discharge, Ann. Glaciol., 53, 229–234, doi:10.3189/2012AoG60A139, 2012.